

Electrochemical properties and separation of Ce in LiF-NaF-KF melt

Authors: Lei, Dr. Min, Qiu, Prof. Jie, Yun, Prof. Di, Zheng, Prof. Bowen, Liu, Prof. Wenguan, Dr. Shaoqiang Guo, Prof. Jie Qiu

Date: 2025-04-08T21:23:04+00:00

Abstract

The electrochemical behavior of Ce(III)/Ce(0) couple in FLiNaK (46.5:11.5:42 mol%) melt was investigated using cyclic voltammetry, chronopotentiometry and square wave voltammetry within the temperature range of 873-933K. Square-wave voltammetry reveals that the reduction of Ce(III) to cerium metal on the inert tungsten electrode is a one-step reduction, i.e. $\text{Ce(III)} + 3\text{e}^- \rightarrow \text{Ce(0)}$. The diffusion coefficient of Ce(III) ion in molten FLiNaK salt, determined via cyclic voltammetry, increases with increasing temperature, and the activation energy of Ce(III) in FLiNaK melt was calculated to be $356.87 \text{ kJ} \cdot \text{mol}^{-1}$. SEM-EDX analysis and XRD patterns results reveal that the pulse electrolysis is a feasible method for Ce separation in molten fluoride salt systems.

Full Text

Preamble

Electrochemical Properties and Separation of Cerium in LiF-NaF-KF Melt

Min Leia, Jie Qiu^{a,†}, Di Yuna, Bowen Zheng^b, Wenguan Li^c, Shaoqiang Guo^{a,*}

a School of Nuclear Science and Technology, Xi'an Jiaotong University, Xi'an 710049, China

b Three Waste Management Institute, China Institute of Radiation Protection, Taiyuan 030000, China

c Sino-French Institute of Nuclear Engineering and Technology, Sun Yat-Sen University, Zhuhai 519082, China

Abstract: The electrochemical behavior of the Ce(III)/Ce(0) couple in FLiNaK (46.5:11.5:42 mol%) melt was investigated using cyclic voltammetry, chrono-

tentiometry, and square wave voltammetry within the temperature range of 873–933 K. Square-wave voltammetry reveals that the reduction of Ce(III) to cerium metal on an inert tungsten electrode occurs as a one-step process, i.e., $\text{Ce(III)} + 3\text{e}^- \rightarrow \text{Ce(0)}$. The diffusion coefficient of Ce(III) ions in molten FLiNaK salt, determined via cyclic voltammetry, increases with temperature, and the activation energy for Ce(III) diffusion in FLiNaK melt was calculated to be $356.87 \text{ kJ} \cdot \text{mol}^{-1}$. SEM-EDX analysis and XRD pattern results demonstrate that pulse electrolysis is a feasible method for cerium separation in molten fluoride salt systems.

Keywords: Electrochemical behavior; FLiNaK salt; Ce(III)/Ce(0); Diffusion coefficient; Electrodeposition

† Corresponding authors: guos2019@xjtu.edu.cn (S. Guo); qiu2021@xjtu.edu.cn (J. Qiu)

1. Introduction

Thorium-uranium cycle-based molten salt reactors have gained significant attention in recent years, with spent fuel processing remaining a key challenge for researchers aiming to enhance the economic efficiency of nuclear energy and improve environmental safety [?, ?]. The thorium-based molten salt reactor system (TMSR) employs fluoride salts as coolant and/or fuel solvent. In TMSR, nuclear fuel is uniformly dissolved in a carrier salt composed of LiF and BeF₂ in the form of fluorides (ThF₄, UF₄, or TRUF), where TRUF refers to transuranic fractions. This design enables the extraction or replenishment of fuel during reactor operation, facilitating both online and offline fuel processing and recycling. After separating uranium and residual components via fluoride volatilization and vacuum distillation of the carrier salt, the resulting molten salt waste (LiF-BeF₂-ThF₄-UF₄-TRUF-FPF) consists primarily of thorium and fission products, where FPF denotes fission product fractions [?]. Among these, Ce, Nd, and Sm are the three elements with the highest concentrations of fission products in spent fuel [?, ?]. Cerium primarily exists in spent nuclear fuel as various radioisotopes, including ¹⁴⁴Ce, ¹⁴⁶Ce, and ¹⁴⁸Ce, which possess extended half-lives (for instance, the half-life of ¹⁴⁴Ce is 285 years). Notably, ¹⁴⁴Ce exhibits significant neutron absorption cross sections, which can adversely affect the neutron economy of reactors or the operational efficiency of transmutation facilities [?]. By isolating and removing radioactive cerium isotopes, the neutron economy of the nuclear fuel cycle can be optimized, thereby significantly mitigating the radiological risks associated with spent fuel reprocessing and final disposal. Moreover, given that cerium coexists with plutonium isotopes and other transuranic elements (such as americium and curium), the separation of cerium represents a critical step in the partitioning and recovery of transuranic elements (TRU), which is essential for fuel reuse.

Since 1959, when Murbach and Hansen proposed an electrolytic refining process for nuclear fuel in molten chlorides [?], researchers have studied the electrolytic

reduction and refining of Ce in chloride molten salts, finding that the diffusion coefficient of Ce(III) in chloride molten salts is relatively high at inert electrodes [?]. Wang et al. investigated the electrochemical, thermodynamic, and kinetic properties of Ce(III) in LiCl-KCl molten salt on an inert tungsten electrode, successfully extracting Ce through constant potential electrolysis and achieving a total purity of 99.971% for metallic Ce [?]. Underpotential deposition alters the reduction potential of metal cations on active electrodes, enabling the extraction of fission products from molten salts using active electrodes. Han et al. studied the electrochemical behavior of Ce(III) on Ni electrodes, revealing that different Ce-Ni intermetallic compounds can be obtained by controlling the applied potential [?]. In 2023, Liu et al. investigated the electrochemical behavior of La(III), Ce(III), and Nd(III) ions in LiCl-KCl-CsCl eutectic salts, finding that the difficulty of cathodic passivation followed the sequence La(III) < Ce(III) < Nd(III) [?]. They also observed that passivation phenomena did not affect the equilibrium potentials of La(III), Ce(III), and Nd(III). In 2024, Xi et al. studied the electrochemical behavior of Ce(III) and found that the diffusion coefficient for Ce(III) was $0.85 \times 10^{-5} \text{ cm}^2/\text{s}$ underpotential deposition; they successfully achieved electrochemical extraction of Ce in LiCl-KCl molten salt by forming a Ce-Zr solid solution, with a recovery rate of 94.02% within 5 hours [?]. To date, the thermodynamic properties of Ce extraction on active electrodes (including Ni [?], Mg [?], Bi [?], Zn [?], Ga [?], and Cd [?]) have been studied, and results show that electro-extraction products result from the reaction $\text{Ce(III)} + 3\text{e}^- + \text{xM} \rightarrow \text{CeM}$, forming M-metallic compounds at the active cathode. However, limited research has been conducted on its kinetic properties.

In recent years, research has been conducted on the fundamental properties of fission products in different molten salt systems [?, ?]. In 2014, Nam et al. used first-principles molecular dynamics modeling to calculate the density, bulk modulus, thermal expansion coefficient, and self-diffusion coefficient of FLiNaK and FLiBe, finding that the obtained data matched experimental data very well [?]. Mushnikov et al. found that in LiF-NaF-KF molten salt, the solubility of CeF_3 is 10 mol.% at 500°C and reaches 25 mol.% at 665°C, showing an increasing trend with rising temperature [?]. However, few studies have investigated the fundamental properties of Ce in fluoride molten salts, and existing research primarily focuses on simulation calculations, which significantly deviate from experimental results. Researchers have suggested that based on differences in the electrochemical and thermodynamic properties of fission products and actinides on active electrodes in molten salts, it is possible to remove radioactive/neutron-absorbing fission products and facilitate the disposal of radioactive waste, such as Ce [?]. However, the accumulation of fission products such as alkali metals, alkaline earth metals, and rare earth elements on electrodes can affect the recovery rate of actinides. Therefore, enhancing the dynamic and thermodynamic research on different fission products (e.g., Ce) in the fluoride molten salt system is of great significance for the treatment and disposal of spent fuel.

This study investigated the redox behavior of Ce(III) on a tungsten electrode

within the temperature range of 873 K to 933 K in the FLiNaK molten salt system. Using cyclic voltammetry and square wave voltammetry, a one-step reduction process of Ce(III) was observed on the tungsten electrode. The diffusion coefficient and apparent standard potential of Ce(III) were systematically measured at different temperatures, with an activation energy calculated to be $356.87 \text{ kJ} \cdot \text{mol}^{-1}$. After four stages of pulsed electrolysis, successful deposition of Ce metal was observed on the surface of the tungsten electrode.

2.1 Materials

A 50 g sample of FLiNaK was prepared in the molar ratio of LiF:NaF:KF (46.5:11.5:42 mol%) and mixed with CeF_3 at a concentration of 3 wt.%. After thoroughly mixing the fluoride powders with a stirrer, the mixture was placed in a 100 mL nickel crucible. All chemicals used in the experiments were purchased from Aladdin: LiF (99.9% purity, metal basis), NaF (99.99% purity, metal basis), KF (99.9% purity, metal basis), and CeF_3 (99.99% purity, metal basis). Subsequently, the fluoride salt mixture was dried at 673 K for 12 hours to remove excess water and oxygen, then heated to the experimental temperature and maintained for 4 hours to reach a steady state for subsequent electrochemical measurements. All operations were carried out in an argon-atmosphere glovebox with water and oxygen content maintained below 1 ppm.

2.2 Measurement of the Electrochemical Properties of Ce(III)

All electrochemical studies were performed using a Gamry electrochemical workstation (Gamry Interface 1010E) based on a conventional three-electrode system. A graphite rod ($\phi 4 \text{ mm} \times 150 \text{ mm}$, Alfa-Aesar) served as the counter electrode (CE), a tungsten wire ($\phi 1.5 \text{ mm} \times 150 \text{ mm}$, Merson) as the working electrode (WE), and a platinum rod ($\phi 1.5 \text{ mm} \times 150 \text{ mm}$, Alfa-Aesar) as the reference electrode (RE). After the FLiNaK salt was melted, the electrodes were inserted into the molten salt to a depth of 7 mm for subsequent electrochemical measurements. Transient techniques including cyclic voltammetry (CV, potential range: 0–2.0 V, scan rate: 0.1–0.6 V/s), chronopotentiometry (CP, current range: –50 to –100 mA), and square wave voltammetry (SWV, scan rate: 0.1 V/s, frequency: 10 Hz, scan range: –1.4 to –1.8 V, pulse size: 25 mV) were employed to characterize the electrochemical properties of Ce(III) in the CeF_3 -FLiNaK molten salt.

2.3 Electrolytic Deposition of Ce

The electrochemical deposition of Ce in the CeF_3 -FLiNaK molten salt system was carried out using a pulsed potentiostatic electrolysis method. Each pulsed electrolysis process consisted of four stages: (1) applying a potential more negative than the deposition potential of Ce(III) for a short duration to locally

concentrate electroactive species on the electrode surface; (2) applying a deposition potential slightly more negative than the precipitation potential of Ce(III) to facilitate Ce deposition; (3) applying a slightly positive voltage to temporarily switch the cathode to an anode, allowing deposited species on the cathode surface to redissolve; and (4) applying a stable voltage to reduce disturbances on the electrode surface, minimizing precipitation and dissolution of Ce between the electrode and bulk molten salt. After electrochemical deposition, samples were removed and characterized using X-ray diffraction (XRD), scanning electron microscopy (SEM), and energy-dispersive spectroscopy (EDS).

2.4 Electrolytic Product Analysis

Following high-temperature pulse electrolysis, a significant amount of electrolytic product accumulated on the working electrode surface. The working electrode was extracted at elevated temperature and allowed to cool naturally before collecting the cathode product. All procedures were conducted within an argon-filled glovebox. X-ray diffraction analysis of the electrolytic products was performed using a Bruker D8 Advance diffractometer equipped with Cu $K\alpha$ radiation ($\lambda = 1.54184 \text{ \AA}$) at 40 kV and 40 mA, with scanning parameters set to a 2θ range of 10° - 80° and a scanning speed of $8^\circ/\text{min}$. The portion of the working electrode containing electrolytic products was vertically positioned in a vacuum-cooled setting mold for solidification. Specifically, 20.03 g of curing agent and 40.24 g of epoxy resin were thoroughly mixed and poured into the mold containing the electrode. After complete resin solidification within the cylindrical mold, the sample was removed and the test surface was polished using an MP-2A polishing machine. Subsequently, the embedded electrode was sectioned, and the electrolytic products on the electrode surface were examined using a GeminiSEM 500 scanning electron microscope coupled with energy-dispersive X-ray spectroscopy (EDS).

3.1 Redox Behavior of Ce in CeF_3 -FLiNaK

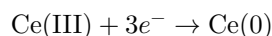
The electrochemical behavior of Ce(III) on a tungsten electrode in CeF_3 (3 wt.%) -FLiNaK molten salt at 873 K was investigated using CV curves, as shown in Fig. 1 Figure 1: see original paper. In the CV curve of the blank salt, represented by the black dashed line, a pair of redox peaks appears around -1.766 V/-1.996 V, corresponding to the Li(I)/Li(0) redox couple. After adding CeF_3 to the FLiNaK salt, a new pair of redox peaks (b/b') was observed around -1.399 V/-1.697 V, associated with the oxidation and reduction of Ce metal. These results indicate that the reduction of Ce(III) to Ce(0) occurs in a single step. Note that the oxidation peak c at -0.894 V may originate from impurities, and the significant rise (d) at the end of the cyclic voltammetry curve corresponds to fluorine gas generation [?]. Impurity peaks and fluorine gas generation were also detected in blank FLiNaK molten salt. Notably, the redox peak for Li(I)/Li(0) exhibited a negative shift of approximately 0.1 V after CeF_3 addition, as shown in Fig. 1(b). This is likely due to the instability of the reference electrode in

FLiNaK, which is confirmed by chronopotentiometric measurements. As presented in Fig. 1(b), a similar offset of about 0.1 V for the reference electrode was observed through chronopotentiometry scanning.

Square wave voltammetry offers higher sensitivity for detecting redox reaction types, and its reversibility and rapid scanning capabilities are advantageous for studying redox kinetics and calculating the number of electrons transferred. Fig. 2 Figure 2: see original paper shows the SWV curve scanned in the low-potential range for the CeF_3 (3 wt.%)–FLiNaK molten salt at a frequency of 10 Hz. From Fig. 1(a), it is evident that signal b' (-1.697 V) corresponds to the reduction of Ce(III) to Ce(0). By focusing on the voltage range where SWV signal b' appears and performing Gaussian fitting, a half-peak width of 0.087 V was obtained, as illustrated in Fig. 2(a). The half-peak width for Ce(III) ions can be used to calculate the number of electrons transferred using the half-peak width formula presented in Equation (1) below [?]:

$$W_{1/2} = \frac{3.52RT}{nF}$$

where $W_{1/2}$ represents the half-peak width, n is the number of electrons transferred, T is the temperature (K), F is the Faraday constant (96485.3383 ± 0.0083 C/mol), and R is the gas constant (8.314 J·mol⁻¹·K⁻¹). The estimated value of n is approximately 3.02, which is close to 3, indicating that the reduction of Ce(III) to Ce(0) involves a one-step, three-electron transfer process, consistent with previous research findings [?, ?, ?]. The electrode reaction for Ce(III)/Ce(0) is described as follows:



3.2 Diffusion Behavior of Ce(III) in FLiNaK Molten Salt System

In electrochemical processes, the diffusion coefficient is a critical parameter because diffusion control typically represents the rate-determining step in most electrode reactions. The diffusion rate directly affects electrolysis efficiency and current efficiency. Therefore, this study conducted detailed measurements of the Ce(III) diffusion coefficient in the molten salt. Fig. 2(b) shows CV curves obtained at different scan rates ranging from 0.1 to 0.6 V/s in CeF_3 (3 wt.%)–FLiNaK molten salt at 873 K. To verify reaction reversibility, the relationship between peak potential and scan rate was plotted, as shown in Fig. 2(c). With increasing scan rate, the reaction progressively transitioned into the diffusion-controlled region. Concentration polarization within the molten salt became more pronounced, leading to a gradual negative shift in the reduction potential and a gradual positive shift in the oxidation potential. Simultaneously, the peak redox current of Ce(III) exhibited a gradual increase. Fig. 2(d) illustrates the

relationship between the peak current and the square root of scan rate, showing a linear correlation between the peak current (I_p) and $v^{1/2}$. This indicates that the reduction of Ce(III)/Ce(0) is a reversible reaction controlled by diffusion. For diffusion-controlled electrochemical reactions, the diffusion coefficient of Ce(III) in molten salt can be calculated using the Berzins and Delahay (B&D) equation, as follows [?]:

$$I_p = 0.61(nF)^{3/2}AC_0\sqrt{D_{\text{Ce(III)}}v}$$

where I_p is the cathodic peak current, n is the number of electrons transferred, T is the absolute temperature (K), A is the effective electrode area (cm^2 , 0.3297 cm^2), C_0 is the initial concentration of CeF_3 (mol/cm^3 , $2.30 \times 10^{-4} \text{ mol}/\text{cm}^3$), $D_{\text{Ce(III)}}$ is the diffusion coefficient (cm^2/s), and v is the scan rate. Using the slope from the linear relationship between cathodic peak current and the square root of scan rate as input to Equation (3), the diffusion coefficient of Ce ions was determined to be $1.95 \times 10^{-7} \text{ cm}^2/\text{s}$.

Typically, due to differences in the degree of cathodic polarization at the electrode, diffusion coefficients can vary significantly. In this study, two different methods were used to calculate diffusion coefficients. The CP test showed a lower degree of cathodic polarization at the electrode, while the CV test exhibited more severe polarization phenomena. Fig. 3(a) presents the CP curve for the CeF_3 (3 wt.%)–FLiNaK molten salt system, in which the current applied to the tungsten electrode varied from -50 to -100 mA. From Fig. 3(a), a distinct redox process can be observed near -1.67 V, corresponding to the redox of Ce(III). The duration of the transition time (τ) of the plateau is related to the magnitude of the current applied to the working electrode, with larger currents resulting in shorter transition times. However, the onset potential for reduction does not change with current, indicating that the electrode reaction is a diffusion-controlled process [?]. These results are consistent with those obtained from the CV method, further corroborating the validity of the CV results. According to the Sand equation (Equation 4 [?]), there is a linear relationship between the applied current in the CP spectrum and $\tau^{-1/2}$ (Fig. 3(b)), which can be used to calculate the diffusion coefficient of Ce(III):

$$I = \frac{0.5nFAC_{\text{Ce(III)}}\sqrt{\pi D_{\text{Ce(III)}}}}{\sqrt{\tau}}$$

where I represents the set current (A), τ is the transition time, n is the number of electrons transferred (3), F is the Faraday constant, A is the electrode area, and $C_{\text{Ce(III)}}$ is the concentration of Ce. Based on the potentiometric graph in Fig. 3(a), the diffusion coefficient of Ce(III) at 873 K was calculated to be $2.15 \times 10^{-6} \text{ cm}^2 \cdot \text{s}^{-1}$. This value is an order of magnitude higher than the diffusion coefficients calculated from CV data and Equation (2) at the same temperature, which is attributed to the lesser degree of electrode polarization during

CP measurements, consistent with observations in other molten salt systems [?]. Based on these results, the diffusion coefficient of Ce(III) in the fluoride salt system is an order of magnitude lower compared to that in chloride salt systems [?]. This is likely attributed to the formation of tight ion pairs (LiF^- , NaF^- , and KF^- , $n = 4-6$) between F^- and small cations, which substantially reduces the concentration of free ions and consequently affects the mobility of rare earth ions. Furthermore, the high concentration and small size of F^- facilitate the development of a highly ordered structure, thereby restricting ion jump pathways, while the absence of effective charge shielding further contributes to elevated migration barriers.

3.3 Diffusion Activation Energy of Ce(III) in FLiNaK Molten Salt

The diffusion coefficients of Ce(III) at various temperatures were also investigated. Despite considerable potential variation in FLiNaK molten salt, the impact of cathode polarization should be minimized. Nevertheless, in FLiNaK molten salt, the Li(I)/Li(0) electrochemical window and transition time exhibit instability with temperature variation. Hence, CV was employed to observe the diffusion coefficient of CeF_3 in FLiNaK salt within the temperature range of 893–933 K, with experimental results shown in Figs. (4–6). Table 1 presents the diffusion coefficients of Ce(III) (i.e., $D_{\text{Ce(III)}}$) in FLiNaK salt at different temperatures, calculated according to the CV curves from Figs. (4–6) and Equation (2). The data in Table 1 reveal that as temperature increases, the redox potential of Ce(III) shifts positively and the diffusion coefficient also increases.

Fig. 4 [Figure 4: see original paper]. (a) Cyclic voltammetry curve of CeF_3 -FLiNaK molten salt at 893 K ($C_{\text{Ce(III)}} = 2.30 \times 10^{-4} \text{ mol/cm}^3$, $A = 0.3768 \text{ cm}^2$); (b) Cyclic voltammetry curve of CeF_3 (3 wt%)-FLiNaK recorded on the tungsten electrode at different scanning rates; (c) E_p and $\log v$ curves; (d) Ratio of the average current to $v^{1/2}$.

Fig. 5 [Figure 5: see original paper]. (a) Cyclic voltammetry curve of CeF_3 -FLiNaK molten salt at 913 K ($C_{\text{Ce(III)}} = 2.30 \times 10^{-4} \text{ mol/cm}^3$, $A = 0.3768 \text{ cm}^2$); (b) Cyclic voltammetry curve of CeF_3 (3 wt%)-FLiNaK recorded on the tungsten electrode at different scanning rates; (c) E_p and $\log v$ curves; (d) Ratio of the average current to $v^{1/2}$.

Fig. 6 [Figure 6: see original paper]. (a) Cyclic voltammetry curve of CeF_3 -FLiNaK molten salt at 933 K ($C_{\text{Ce(III)}} = 2.30 \times 10^{-4} \text{ mol/cm}^3$, $A = 0.3768 \text{ cm}^2$); (b) Cyclic voltammetry curve of CeF_3 (3 wt%)-FLiNaK recorded on the tungsten electrode at different scanning rates; (c) E_p and $\log v$ curves; (d) Ratio of the average current to $v^{1/2}$.

Table 1. Redox potential and diffusion coefficient of Ce(III) in FLiNaK salt at different temperatures calculated from CV curves.

Temperature	Redox Potential	Diffusion Coefficient
873 K	-1.401 V / -1.694 V	1.95×10^{-7} cm ² /s
893 K	-1.376 V / -1.664 V	5.88×10^{-7} cm ² /s
913 K	-1.317 V / -1.556 V	1.35×10^{-6} cm ² /s
933 K	-1.342 V / -1.607 V	4.98×10^{-6} cm ² /s

The influence of temperature on diffusion processes in an electrolyte typically follows the Arrhenius equation [?], which expresses the relationship between the diffusion coefficient D and temperature T as follows:

$$D = D_0 \exp\left(-\frac{E_a}{RT}\right)$$

where E_a is the activation energy for diffusion ($\text{J} \cdot \text{mol}^{-1}$), R is the gas constant, and D_0 is the pre-exponential factor. The diffusion coefficient D ($\text{cm}^2 \cdot \text{s}^{-1}$) is related to $1/T$ (K^{-1}) in an exponential manner. The activation energy E_a for the diffusion process can be obtained from the slope of the following linear relationship:

$$\ln D = \ln D_0 - \frac{E_a}{RT}$$

Based on the experimental results in Table 1 and Equation (6), the activation energy for diffusion of Ce(III) in the FLiNaK molten salt system was determined to be $356.87 \text{ kJ} \cdot \text{mol}^{-1}$, as shown in Fig. 7 [Figure 7: see original paper]. This value is significantly higher than the activation energy ($30.8 \text{ kJ} \cdot \text{mol}^{-1}$) in the chloride CeF_3 -LiCl-KCl system [?], indicating that the FLiNaK salt system may have stronger ionic interactions that require more energy to overcome during diffusion.

Fig. 7. Arrhenius plot of the logarithm of the diffusion coefficient (D) of Ce in molten FLiNaK salt versus the reciprocal of temperature ($1/T$).

3.4 Apparent Standard Potential

The apparent standard potential is an important thermodynamic parameter for studying the electrochemical reactivity of ions in molten salts. It serves as an indicator of the electrochemical properties and oxidizing or reducing ability of a substance at a given electrode. A more positive potential indicates stronger oxidizing ability in its oxidized state, while a more negative potential signifies stronger reducing ability in its reduced state. Additionally, differences between standard potentials can be used to determine whether substances can be separated via electrolysis. However, most molten salt systems deviate from standard conditions, resulting in a lack of available standard potential databases. Due to the presence of nucleation overpotential, transient electrochemical techniques

are not suitable for determining the apparent standard potential of the system. In this study, the electromotive force measurement method was employed to determine the apparent standard potential [?]. At different temperatures, a cathodic current was applied to the tungsten electrode for 60 seconds to deposit metallic Ce, and the open circuit potential (OCP) was recorded against a Pt reference electrode, producing a stable plateau corresponding to the equilibrium potential E_{eq} .

Since the standard electrode potential E^0 has the following relationship with the equilibrium potential E_{eq} and the apparent standard electrode potential E^{*0} [?]:

$$E_{\text{Ln}(n)/\text{Ln}(0)} = E_{\text{Ln}(n)/\text{Ln}(0)}^0 + \frac{RT}{nF} \ln \left(\frac{a_{\text{Ln}(n)}}{a_{\text{Ln}(0)}} \right)$$

$$E_{\text{Ln}(n)/\text{Ln}(0)} = E_{\text{Ln}(n)/\text{Ln}(0)}^{*0} + \frac{RT}{nF} \ln (X_{\text{Ln}(n)} \gamma_{\text{Ln}(n)})$$

where n , R , T , and F are defined as in previous equations; $E_{\text{Ln}(n)/\text{Ln}(0)}^0$ represents the standard potential; $X_{\text{Ln}(n)}$ and $\gamma_{\text{Ln}(n)}$ represent the concentration and activity coefficient of Ln(n) ions, respectively; and Ln metal $\alpha_{\text{Ln}(0)}$ has an activity of 1. Combining formulas (7) and (8), we obtain the following relationship:

$$E_{\text{Ln}(n)/\text{Ln}(0)} = E_{\text{Ln}(n)/\text{Ln}(0)}^{*0} + \frac{RT}{nF} \ln (X_{\text{Ln}(n)} \gamma_{\text{Ln}(n)})$$

Typically, the equilibrium potential in molten salts can be determined by measuring the OCP. At different temperatures, a negative current was continuously applied to the tungsten electrode for 60 s, and the OCP relative to the reference electrode was recorded. As shown in Fig. 8 [Figure 8: see original paper], each experiment yields a potential plateau, where the plateau region corresponds to the equilibrium potential of Ce(III)/Ce at different temperatures relative to the Pt reference electrode. Subsequently, using Equation (8), the apparent standard electrode potentials of Ce(III)/Ce relative to Pt at different temperatures were calculated, with results presented in Table 2. Table 2 shows that as temperature increases, the measured apparent standard potential shifts positively, indicating a decreasing absolute potential value. This temperature dependence is consistent with the Nernst equation, which states that electrode potential is positively correlated with temperature [?].

Fig. 8. Open circuit potential obtained after applying a negative current for 60 s to CeF₃-FLiNaK molten salt on a tungsten electrode.

Table 2. Apparent standard potential of Ce(III)/Ce pairs in molten FLiNaK salt calculated from OCP results.

Temperature	E_{eq} (vs. Ref)	E^{*0} (vs. Ref)
873 K	-1.564 V	-1.486 V
893 K	-1.340 V	-1.313 V
913 K	-1.773 V	-1.699 V
933 K	-1.558 V	-1.536 V

3.5 Electrolytic Separation of Ce in CeF_3 (5 wt.%)-FLiNaK

The above results (Section 3.1) indicate that in the CeF_3 (5 wt.%)-FLiNaK molten salt system, Ce(III) can be reduced to metallic Ce through a one-step, three-electron transfer electrochemical reaction, suggesting feasibility for Ce separation via electrolysis. To verify this feasibility, preliminary electrolysis experiments were conducted. As electrolysis progresses, the concentration of the electroactive Ce(III) ion in the molten salt system continuously decreases. Furthermore, during electrolysis, molten salt can adhere to the electrode surface along with electrolysis products, which somewhat impedes further Ce(III) deposition. To overcome the decrease in Ce(III) concentration and reduction in current efficiency caused by molten salt adhesion, pulsed electrochemical methods were employed. The pulsed potential electrolysis method can effectively mitigate the impact of reactive ion concentration changes, thereby improving current efficiency. Fig. 9 Figure 9: see original paper illustrates the voltage cycle for the pulsed potential electrolysis method used in this study. Each pulse cycle lasted 65 s and consisted of four stages: (1) applying a potential of -1.7 V, which is between the reduction potential of Li^+ (-2.0 V vs. Pt) and the reduction potential of Ce(III) (-1.65 V vs. Pt), for 5 s to allow Ce(III) to concentrate on the cathode surface; (2) applying a potential of -1.67 V, slightly more negative than the reduction potential of Ce(III), for 55 s to selectively deposit Ce; (3) applying a positive potential of 0.3 V for 3 s to redissolve the loose layer on the surface of the deposited phase back into the molten salt; and (4) applying zero potential for 2 s to maintain the molten salt system in a stable state.

The electrolysis process was carried out for a total of 100 cycles, as shown in Fig. 9(b). Throughout the electrolysis process, the current remained relatively constant, indicating that ion concentration changes resulting from electrolysis had no significant impact on the pulse potential electrolysis process. Since the concentration and current density of Ce(III) near the electrode were relatively stable, fluctuations in electrode potential caused by concentration polarization were small, reducing the likelihood of side reactions and impurity deposition.

Fig. 9. (a) Experimental parameters for pulse potential electrolysis of CeF_3 (5 wt.%)-FLiNaK molten salt system; (b) Change in current with time during pulse potential electrolysis of CeF_3 (5 wt.%)-FLiNaK molten salt system at 873 K, working electrode: tungsten, 4 mm.

CV tests were conducted on the molten salt system before and after electrolytic separation, with results shown in Fig. 10 [Figure 10: see original paper]. After

electrolysis, the Li^+ and impurity peaks shifted upward by about 62 mV, and the corresponding oxidation-reduction peak for $\text{Ce(III)} \rightarrow \text{Ce(0)}$ was significantly reduced, indicating that part of the Ce(III) in the molten salt was electrolytically separated. Since peak current in CV curves is related to concentration, the effect of electrolytic separation can be estimated by the ratio of cathodic peak currents (I_{pc}) corresponding to $\text{Ce(III)} \rightarrow \text{Ce(0)}$ measured before and after electrolysis under identical conditions. The ratio obtained from Fig. 10 is $I_{pc,\text{front}}/I_{pc,\text{back}} = -0.06854 \text{ V} / -0.02448 \text{ V} = 2.80$, indicating that the Ce(III) concentration in the molten salt decreased by approximately 2.8 times after electrolysis.

Fig. 10. Cyclic voltammetry curves before and after electrolysis in molten FLiNaK, scan rate: 200 mV/s, temperature: 873 K. Note: a/a' refers to $\text{Li}^+ + \text{e}^- = \text{Li}$; b/b' refers to $\text{Ce}^{3+} + 3\text{e}^- = \text{Ce}$; c refers to impurity; d refers to F_2 .

After electrolytic separation, the cathode product was identified using XRD, with results shown in Fig. 11 [Figure 11: see original paper]. The analysis reveals that Ce exists primarily in metallic form in the electrolysis product, with a small amount of CeF_3 signal also present. Signals for LiF, KF, and NaF in the spectrum originate from contamination during sample collection and transfer, where molten material was exposed. KF is easily hydrated during transfer, so $\text{KF} \cdot 2\text{H}_2\text{O}$ signals also appear in the spectrum.

Fig. 11. XRD patterns of separation products after pulsed potential electrolysis in molten FLiNaK salt.

The cross-section of the working electrode after electrolytic separation was characterized using EDS. As shown in Fig. 12 [Figure 12: see original paper], the protruding electrolysis products exhibit a distinct metallic luster and Ce enrichment. Note that the shaded area at the bottom of the SEM image represents the tungsten rod (i.e., working electrode). Similarly, EDS mapping spectral analysis revealed significant Na, K, and Ce elements in the products, consistent with XRD results. Combined with XRD and EDS findings, these results demonstrate that pulse electrolysis is a feasible method for Ce separation in molten fluoride salt systems.

Fig. 12. Cross-sectional SEM image and corresponding EDS maps of the working electrode after pulsed potential electrolysis in molten FLiNaK salt.

4 Conclusions

The electrochemical behavior of Ce(III) in the CeF_3 (3 wt.%)–FLiNaK molten salt system was studied using cyclic voltammetry, chronopotentiometry, and square wave voltammetry. The main findings are as follows: (1) Square-wave voltammetry reveals that the reduction of Ce(III) to cerium metal on an inert tungsten electrode is a one-step reduction, i.e., $\text{Ce(III)} + 3\text{e}^- \rightarrow \text{Ce(0)}$, representing a quasi-reversible reaction process controlled by diffusion. (2) The diffusion coefficient of Ce(III) ions in molten FLiNaK salt, determined via cyclic

voltammetry, increases with temperature, and the activation energy for Ce(III) diffusion in FLiNaK melt was calculated to be $356.87 \text{ kJ} \cdot \text{mol}^{-1}$. (3) Compared with chloride salt systems, the high concentration of free F^- in fluoride salt systems has a pronounced effect on the molten salt medium, readily forming complex clusters with metal ions and affecting the diffusion coefficient. (4) The apparent standard potential gradually shifts positively with increasing temperature, with the absolute potential value becoming progressively smaller. (5) The CeF_3 -FLiNaK molten salt system was electrolyzed using a four-stage pulse potential electrolysis method for 1.8 h, resulting in a significant decrease in Ce concentration in the molten salt. This preliminary study demonstrates that pulse electrolysis is a feasible method for Ce separation in molten fluoride salt systems.

Acknowledgements: This work was financially supported by the Research Project of Shaanxi Province (Grant No. 2023SYJ18) and the Natural Science Basic Research Project of Shaanxi Province (Grant No. 2023-JC-QN-0419).

5 References

- [1] M. Lung, O. Gremm, Perspectives of the thorium fuel cycle, *Nuc. Eng. Des.* 180(1998) 133-146.
- [2] J. Serp, M. Allibert, O. Beneš, S. Delpech, O. Feynberg, V. Ghetta, D. Zhimin, The molten salt reactor (MSR) in generation IV: Overview and perspectives, *Prog. Nucl. Energy.* 77(2014) 308-319.
- [3] G. Y. Zhou, M. Wu, C. Bao, N. Zhang, S. T. Tu, Structural optimization of gas-solid separator used in TMSR-SF based on computational fluid dynamics, *Nucl. Eng. Des.* 421(2024) 113097.
- [4] W. Gong, X. Wang, C. Huang, X. Wang, Y. Fu, Layout optimization for the high-temperature nuclear loop with movable equipment based on TMSR-LF1, *Ann. Nucl. Energy.* 199(2024) 110362.
- [5] Z. Zhao, J. Geng, Z. Cheng, W. Li, Q. Dou, L. Zhang, Q. Li, Control and surveillance of redox potential for ^{233}Pa dissolution in $2\text{LiF}-\text{BeF}_2$ molten salt, *RSC adv.* 14(2024) 15994-16000.
- [6] A. A. Lizin, S. V. Tomilin, O. E. Gnevashov, R. K. Gazizov, A. G. Osipenko, M. V. Kormilitsyn, A. A. Baranov, L.V. Zaharova, V.S. Naumov, L.I. Ponomarev, PuF_3 , AmF_3 , CeF_3 , and NdF_3 solubility in $\text{LiF}-\text{NaF}-\text{KF}$ melt, *At. Energy.* 115(2013) 11-17.
- [7] J. Bruno, R. C. Ewing, Spent nuclear fuel, *Elements.* 2(2006) 343–349.
- [8] S. A. Kuznetsov, A. V. Popova, Y. V. Stulov, S. I. Markovich, Electrochemistry of Neodymium in an Equimolar $\text{NaCl}-\text{KCl}$ Melt without and with Addition of Fluoride Ions, *J. Elec. Soc.* 170(2023) 076508.
- [9] E. W. Murbach, W. N. Hansen, Pyroprocessing thorium fuels, *J. Ind. Eng. Chem.* 51(1995) 177-178.
- [10] X. Xi, J. Wang, J. Zhang, W. Li, S. Ning, T. Jiang, Electrochemical behavior and separation of Ce(III) in $\text{LiCl}-\text{KCl}$ molten salt, *Sep. Purif. Technol.* 334(2024) 125931.

- [11] K. Jiang, Y. Shao, V. Smolenski, A. Novoselova, Q. Liu, M. Xu, J. Wang, Electrochemical study of reduction Ce(III) ions and production of high purity metallic cerium by electrorefining in fused LiCl-KCl eutectic, *J. Electroanal. Chem.* 878(2020) 114691.
- [12] S. Wang, M. Li, W. Han, M. Zhang, W. Wang, Y. Sun, Selective formation of Ce-Ni hydrogen storage alloys by electro-deposition in LiCl-KCl-CeCl₃ melts using Ni as cathode. *J. Alloys Compd.* 777(2018) 1211-1221.
- [13] Y. Liu, Y. Liu, L. Wang, S. Jiang, D. Wang, Z. Liu, W. Shi, Electrochemical Behaviors and Extraction of Ln(III) (Ln = La, Ce, Nd) Ions in LiCl-KCl-CsCl Eutectic Salts at Low Temperatures. *ACS Sustain. Chem. Eng.* 11(2023) 8161-8172.
- [14] M. Zhang, H. Wei, M. Zhang, Z. Fengyan, X. Yun, Z. Zhang, Electrochemical formation process and phase control of Mg-Li-Ce alloys in molten chlorides. *Rare Earths* 31(2013) 609-615.
- [15] B. K. Kim, B. G. Park, Characterization of Ce-Bi intermetallic compound formations by electrolytic reduction in molten LiCl-KCl eutectic. *Electroc. Acta.* 295(2019) 270-277.
- [16] L. Wang, Y. L. Liu, K. Liu, S. L. Tang, L. Y. Yuan, T. Lu, W. Q. Shi, Electrochemical extraction of cerium by forming Ce-Zn alloys in LiCl-KCl eutectic on W and liquid Zn electrodes. *J. Electrochem. Soc.* 2015. 162(2015) 179-184.
- [17] K. Liu, Y.L.Liu, Z.F. Chai, W.Q. Shi, Evaluation of the electroextractions of Ce and Nd from LiCl-KCl molten salt using liquid Ga electrode, *J. Electrochem. Soc.* 164(2017) 169-178.
- [18] D. Yoon, S. Phongikaroon, J. Zhang, Electrochemical and thermodynamic properties of CeCl₃ on liquid cadmium cathode (LCC) in LiCl-KCl eutectic salt. *J. Electrochem. Soc.* 163(2016) 97-103.
- [19] P. Masset, R.J. Konings, R. Malmbeck, J. Serp, J.P. Glatz, Thermochemical properties of lanthanides (Ln = La, Nd) and actinides (An = U, Np, Pu, Am) in the molten LiCl-KCl eutectic, *J. Nucl. Mater.* 344 (2005) 173.
- [20] M. H. Joo, S. J. Park, S. M. Hong, C. K. Rhee, Y. Sohn, Electrochemical Recovery and Behaviors of Rare Earth (La, Ce, Pr, Nd, Sm, Eu, Gd, Tb, Dy, Ho, Er, Tm, and Yb) Ions on Ni Sheets, *Mater.* 13(2020) 5314.
- [21] C. P. Fabian, V. Luca, P. Chamelot, L. Massot, C. Caravaca, G. R. Lumpkin, Experimental and Simulation Study of the Electrode Reaction Mechanism of La³⁺ in LiCl-KCl Eutectic Molten Salt, *J. Electrochem. Soc.* 2012. 159(2012) F63-F67.
- [22] H. O. Nam, A. Bengtson, K. Vörtler, S. Saha, R. Sakidja, D. Morgan, First-principles molecular dynamics modeling of the molten fluoride salt with Cr solute, *J. Nucl. Mater.* 449(2014) 148-157.
- [23] P. N. Mushnikov, O. Tkacheva, A. S. Kholkina, Y. P. Zaikov, V. Y. Shishkin, A. V. Dub, Phase Diagram of the Quasibinary System LiF-NaF-KF-CeF₃, *Atomic Energy*, 131(2022) 263-267.
- [24] W. Li, X. Zhang, J. Wang, L. Chen, Q. Sun, W. Han, Y. Wei, Electrochemical properties and extraction of Dy on liquid Sn electrode in LiCl-KCl molten salt, *J. Solid. State. Electr.* 27(2023).
- [25] Q. Yang, J. Ge, Y. Wang, J. Zhang, Electrochemical Separation of Lan-

- thanum Oxide in Molten FLiNaK Salt. Nucl. Technol. 206(2020) 1769-1777.
- [26] P. Dauphin-Ducharme, N. Arroyo-Currás, M. Kurnik, G. Ortega, H. Li, K. Plaxco, Simulation-based approach to determining electron transfer rates using square-wave voltammetry, Langmuir, 33(2017) 4407-4413.
- [27] N. D. Smith, S. Lombardo, S. L. Shang, Z. K. Liu, H. Kim, Determination of Kinetic Properties of Ni(II) Ions in Molten LiF-NaF-KF via Voltammetry. J. Electrochem. Soc. 170(2023) 066505.
- [28] F. Lantelme, Y. Berghoute, Electrochemical studies of LaCl_3 and GdCl_3 dissolved in fused LiCl-KCl. J. Electrochem. Soc. 146(1999) 4137.
- [29] A. Mehta, G. C. Barker, The dynamics of sand, Rep. Prog. in Phys, 57(1994) 383.
- [30] K.J. Laidler, The development of the Arrhenius equation, J. chem. Education, 1984. 61(1984) 494.
- [31] Z. Liu, G. Lu, J. Yu, Investigation on electrochemical behaviors of Ni(II) impurity in LiCl-KCl melt. Sep. Purif. Technol. 268(2021) 118354.
- [32] S. P. Fusselman, J.J.Roy, D. L. Grimmett, L. F. Grantham, C. L. Krueger, C. R. Nabelek, T. S. Storvick, S. P. Fusselman, Thermodynamic Properties for Rare Earths and Americium in Pyropartitioning Process Solvents. J. Electrochem. Soc. 146(1999) 2573-2580.

Note: Figure translations are in progress. See original paper for figures.

Source: ChinaXiv – Machine translation. Verify with original.